Jodie Scrimshaw S3823172 March 27, 2024

Computational Fluid Dynamics (CFD) analysis of injection moulding dog bones

Supervisor: Pablo Druetta

Second reader: Daniele Parisi

Abstract

This study evaluates the performance of phase field (PF) and level set (LS) methods in simulating the injection moulding process, focusing on mould filling dynamics under varying pressures and viscosities. While higher viscosities were expected to slow down the filling process, this trend was only significant at the highest viscosity tested. The PF method exhibited numerical instability at high pressure and viscosity, unlike the LS method, which remained stable. The PF simulations showed a more structured and uniform filling pattern, whereas the LS method displayed air pockets and a less consistent filling. The study suggests the need for a broader range of viscosity values in future research and indicates that the choice between PF and LS methods should be based on the specific requirements of the moulding process, considering the trade-offs between stability and filling uniformity. The simulation results from heat transfer, influenced by an arbitrary heat flux setting of -100 W m^{-2}, show unrealistic temperature distributions, including negative Kelvin values, indicating the model's current insufficiency for meaningful interpretation in the context of injection moulding thermal dynamics. For future research other modules from COMSOL should be utilized.

Contents

1. Introduction

Computational fluid dynamics (CFD) is a critical tool in the simulation and analysis of fluid flows. Its importance spans across various industries and applications, offering insights that are pivotal for design, optimization, and understanding complex fluid interactions. COMSOL [1] is a computational fluid dynamics (CFD) programme that can be used to simulate and analyse fluid flow for the reasons given. Injection moulding is one major industry where CFD can be of importance. Injection moulding is a process where molten plastic is injected into a mould cavity via an extruder under extremely high pressures and temperatures. The flow behaviour of plastic inside these various moulds are largely unknown and the industry relies on previous empirical data for the optimal processing parameters. Injection moulding is one of the most challenging processing techniques because the outcome of the moulded plastic is highly dependent on processing conditions (temperature, pressure, cooling time, moisture content of plastics, etc.), external factors such as humidity, temperature of the factory, concentration of dust particles, etc., and the nature of the polymer itself. Because of the large number of variables which all can have a significant impact on the final product, this makes introducing novel plastics especially challenging since the industry cannot rely on previous empirical data for optimal processing conditions. A very common mould that is used is the dog bone mould, as dog bones are used to test a plastics mechanical properties such as tensile strength, young's modulus, elongation, etc. This project aims to simulate the injection flow of a molten plastic inside a dog bone mould to discover how varying viscosities and injection pressures affects the filling of the mould. Multiple aspects will be analysed that are of importance in industry such as filling time, filling percentage, flow rate into the mould, flow rate of air leaving the mould, and lastly observing cooling effects as polymer enters the mould. These insights are crucial for mould design and setting processing parameters.

2. Theory

2.1. Polymer viscosity

The Vogel-Fulcher-Tammann equation is used to describe the viscosity of liquids as a function of temperature and specifically in the supercooled regime, upon approaching the glass transition. The equation is shown in (1) [2].

$$\eta = \eta_0 \cdot \frac{B}{e^{T-T_{VF}}} \qquad (1)$$

The values η_0, B, and T_{VF} are empirically determined parameters. The parameters are also dependent on the molecular weight of the polymer, and a number of different parameters can be found for varying molecular weights [2].

2.2. Physics

In this section, the equations governing the two phased fluid flow through the geometric domain will be defined along with the boundary conditions. Computational Fluid Dynamics involves solving the Navier-Stokes equation, which satisfies the conservation of mass, momentum, and energy to predict flow behaviour. The Level Set method (LS) and the Phase Field method (PF) are numerical tools for interface tracking in computational simulations. LS method implicitly captures interfaces and is advantageous for advective-dominated problems, requiring re-initialization to maintain stability. PF method uses a diffuse interface approach, suitable for capturing phase transitions and modelling surface tension naturally but may involve more complex numerics due to additional equations. In this section, a comparison between these two methods will be made. The comparison is critical as it guides the selection of the appropriate method for accurate and efficient simulations of multiphase flows and interfacial dynamics.

2.2.1. Laminar flow

The fluid flow used in this model is incompressible laminar flow. The relevant equations is given in equation (2), which represents the Navier-Stokes equation for incompressible flow [3] with no time dependence for velocity. ρ is the fluid density, $\mathbf{u}$ is the velocity field of the fluid, ∇ is the divergence operator (which measures the rate at which the fluid is expanding or compressing at a point in space), p is the pressure field within the fluid, $\mathbf{K}$ represents the stress tensor (which accounts for the viscous stresses in the fluid, full expression is provided in equation (3), $\mathbf{F}_{\mathrm{ST}}$ represents external forces acting on the fluid, that is the surface tension in this case, and $\mathbf{I}$ is the identity tensor [3].

$$\rho(\mathbf{u}\cdot\nabla)\mathbf{u} = \nabla\cdot[-p\mathbf{I}+\mathbf{K}] + \mathbf{F}_{\mathrm{ST}} \qquad (2)$$

For the stress tensor $\mathbf{K}$ given by equation (3), where μ is the dynamic viscosity.

$$\mathbf{K} = \mu(\nabla\mathbf{u} + (\nabla\mathbf{u})^{\mathrm{T}}) \qquad (3)$$

The continuity equation is given in (4), which states that there is no net flow of mass in or out of any volume within the fluid and therefore it is incompressible [4].

$$\rho\nabla\cdot\mathbf{u} = 0 \qquad (4)$$

Equation (5) specifies the boundary conditions for the inlet, which in this case is the static pressure. $\mathbf{n}$ = the boundary normal point out of the domain, p is pressure in the system, p_0 is the prescribed inlet static pressure, and $\hat{p}_0$ is the average pressure across the boundary. Equation (6) describes that the total pressure at the boundary is always equal or greater than the prescribed pressure. In equation (7) $\mathbf{t}$ is the tangential velocity, and $\mathbf{u}$ is the field velocity, this equation describes that the inflow velocity is only flowing in one direction. The velocity of the fluid in contact with the wall is zero, i.e. $\mathbf{u} = 0$, fulfilling the no-slip condition.

$$\mathbf{n}^{\mathrm{T}}[-p\mathbf{I} + \mathbf{K}]\mathbf{n} = -\hat{p}_0 \qquad (5)$$

$$\hat{p}_0 \geq p_0 \qquad (6)$$

$$\mathbf{u} \cdot \mathbf{t} = 0 \qquad (7)$$

2.2.2. Phase field

Phase field models are used to simulate the interface between two phases, like liquid and gas, and are particularly useful for capturing complex interface dynamics like droplet formation or wetting phenomena. Equation (8) and equation (9) describe the phenomena for the wetted wall where θ_w is the contact angle for the fluid along the wetted wall (the mass flow across the contact angle is zero), γ is surface tension coefficient, λ is the mixing energy density, ϵ_{pf} is the parameter controlling interface thickness, ϕ is the phase field variable that defines the fluid (either -1 or 1), $\nabla\psi$ represents the gradient of the phase field variable ψ (which describes the order parameter of the system, varying smoothly from one phase to another), $|\nabla\phi|$ is the magnitude of the gradient of the phase field variable ϕ [1].

$$\mathbf{n} \cdot \frac{\gamma\lambda}{\epsilon_{pf}^2}\nabla\psi = 0 \qquad (8)$$

$$\mathbf{n} \cdot \epsilon_{pf}^2\nabla\phi = \epsilon_{pf}^2\cos(\theta_w)\,|\nabla\phi| \qquad (9)$$

2.2.3 Multiphysics: Two-Phased Flow, Phase Field

The surface tension force term in equation (2) is calculated using equation (10). Where $\frac{\partial f}{\partial \phi}$ is the phi-derivative of external free energy. The expression $\frac{\lambda}{\epsilon_{pf}^2}\psi$ is the chemical potential, otherwise denoted as G. $\nabla\phi$ is the gradient of the phase field variable [5].

$$\mathbf{F}_{st} = \left(\frac{\lambda}{\epsilon_{pf}^2}\psi - \frac{\partial f}{\partial \phi}\right)\nabla\phi \qquad (10)$$

2.2.4. Level Set

The level set method is a technique in numerical analysis for tracking and analysing interfaces and shapes. The level set variable ϕ is a step function that equals zero in one domain and one in the other. Across the interface there is a smooth transition from zero to one [6]. In equation (11), in the left side, we find terms that are responsible for the accurate progression of the interface, whereas the right side contains terms that are essential to maintaining the numerical robustness of the solution. The parameter denoted by ϵ_{ls} is influential in setting the width of the transition zone where the variable smoothly transitions from zero to one. The parameter γ plays a role in the reinitialization or the stabilization process of the level set function and should be adjusted for each unique scenario [6].

$$\frac{\partial \phi}{\partial t} + \mathbf{u} \cdot \nabla \phi = \gamma \nabla \cdot \left(\epsilon_{ls} \nabla \phi - \phi(1-\phi) \frac{\nabla \phi}{|\nabla \phi|} \right) \qquad (11)$$

2.2.4. Multiphysics: Two-Phased Flow, Level Set

This section describes the surface tension force term in equation (2). It is calculated using equation (12) where σ is the surface tension, $\mathbf{n}_{\mathrm{int}}$ is the unit normal to the interface, κ is the curvature, δ is a Dirac delta function located at the interface, and ∇_s is the surface gradient operator [5]. The expressions for κ and ∇_s are given in equation (13) [5].

$$\mathbf{F}_{\mathrm{st}} = \sigma \delta \kappa \mathbf{n}_{\mathrm{int}} + \delta \nabla_s \sigma \qquad (12)$$

$$\kappa = -\nabla \cdot \mathbf{n}_{\mathrm{int}} \; ; \; \nabla_s = \left(\mathrm{I} - \mathbf{n}_{\mathrm{int}} \mathbf{n}_{\mathrm{int}}^{\mathrm{T}} \right) \nabla \qquad (13)$$

2.2.5. Heat Transfer in Fluids

This section describes the equations governing the heat transfer of the fluids. The Heat Transfer in Fluids Interface solves equation (14) where ρ is the density, C_p is the specific heat capacity, T is the absolute temperature, $\mathbf{u}$ is the velocity vector, $\mathbf{q}$ is the heat flux by conduction, Q contains heat sources other than viscous dissipation, Q_p is the work done by pressure changes, Q_{vd} is the viscous dissipation in the fluid [7].

$$\rho C_p \mathbf{u} \cdot \nabla T + \nabla \cdot \mathbf{q} = Q + Q_p + Q_{\mathrm{vd}} \qquad (14)$$

Equation (15) gives the expression for the heat flux by conduction, where k is the thermal conductivity and T is the temperature.

$$\mathbf{q} = -k \nabla T \qquad (15)$$

Equation (16) is the boundary condition which stats that there is a heat sink or source embedded in the boundary. Where Q_{b} is the heat source which can be negative to make it a heat sink. $\mathbf{n}$ is the vector normal to the boundary.

$$-\mathbf{n} \cdot \mathbf{q} = Q_{\mathrm{b}} \qquad (16)$$

3. Method

This section describes how the model geometry and how it was made, which materials were used in the simulation and the properties of the materials, the setup of the simulation in COMSOL with boundary and initial condition values, and the mesh study.

3.1. Model Geometry

This section explains the selection and development of the dog bone model used in the Computational Fluid Dynamics (CFD) simulation. In the development of the simulation model for the injection moulding process, a dog bone-shaped specimen conforming to the dimensional specifications of ASTM D638 Type I and ISO 527 standards was utilised. This adherence to recognized international standards ensures the reliability and comparability of the test results. The ASTM D638 Type I specification dictates the geometry of the test specimen, particularly suited for thin plastic materials, with precise requirements for length, width, and thickness, especially in the narrower section where tensile stress is concentrated. The model of the dog bone mould was replicated in SolidWorks [8] using a blueprint obtained from the company Axxicon [9]. The blueprint used is provided in Figure 1 (left).

The dimensions that are not part of the dog bone shape were estimated, such as the runner, the size of the inlet, and gate size. These dimensions do not have standard conventions and are designed based on the specific polymer that will be used in injection moulding. Some polymers such as those that contain fibres or are very viscous require larger dimensions. The rate of cooling and crystallization of polymers also need to be taken into account as the polymer should not start crystallizing in the runner. The dimensions should not be too large as to have excess waste.

The runner is estimated to have a width of 3 mm and a depth of 4.5 mm, which is slightly larger than the dog bone's depth of 3.2 mm. The inlet radius is 3 mm. The air vent outlet is 6 mm wide, 0.02 mm deep, and extends 2 mm outward. Air vents are necessary to remove the air from the mould as the polymer is injected. The air vent should be small enough to prevent any polymer from escaping. The final model created in SolidWorks is shown in Figure 1 (right).

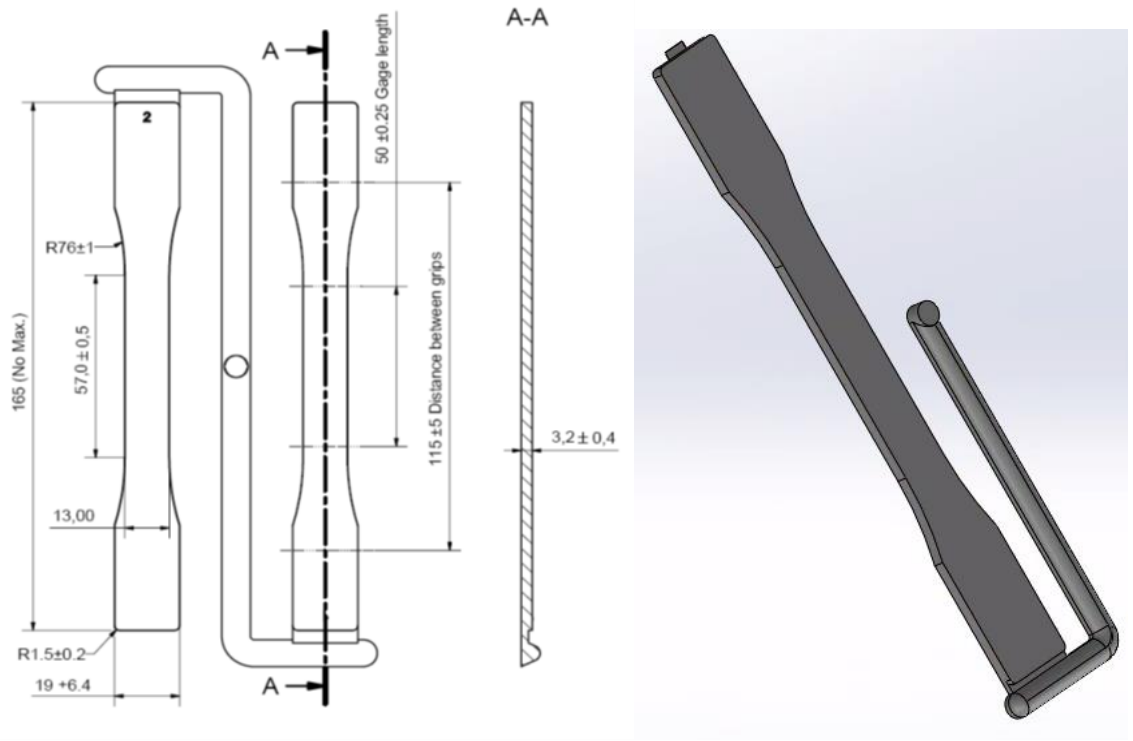

Figure 1: Specimen Design of ASTM D638 TYPE I dog bone mould from Axxicon [9] (left). 3D model of the dog bone mould developed in SolidWorks [8] (right).

3.2. Materials

The polymer chosen to fill the mould in this study is polystyrene. To simulate polystyrene in COMSOL the water material was chosen and only the density and viscosity was changed. The density of polystyrene melt is 945 kg/m^3 [10]. As was shown in the theory section, the viscosity of polystyrene melt is heavily dependent on temperature. For simplicity and computational cost considerations, a viscosity of 1, 2, and 5 Pas is chosen. For more accurate results, the VFT equation with relevant parameters explained in the theory section should be chosen as well as changing the material to a non-Newtonian fluid. The other material is air and chosen from the COMSOL materials library.

3.3 Boundary conditions

3.3.1. Laminar Flow

The volume is initially occupied solely with air, and the inlet will only have inflow of polymer. Backflow is supressed to prevent fluid exiting the domain through the inlet boundary. For the wall, there is a no slip condition i.e. $\mathbf{u} = 0$. Outlet static pressure of p_0 = 0 bar is set. Inlet pressure is static and set using a step function to prevent numerical instability i.e. P_inlet*step1(t). P_inlet is a

variable that is defined as either 500 bar, 600 bar or 700 bar. The step function is from 0 to 1, with location at 0.2 and a transition zone of 0.5 (Figure 2).

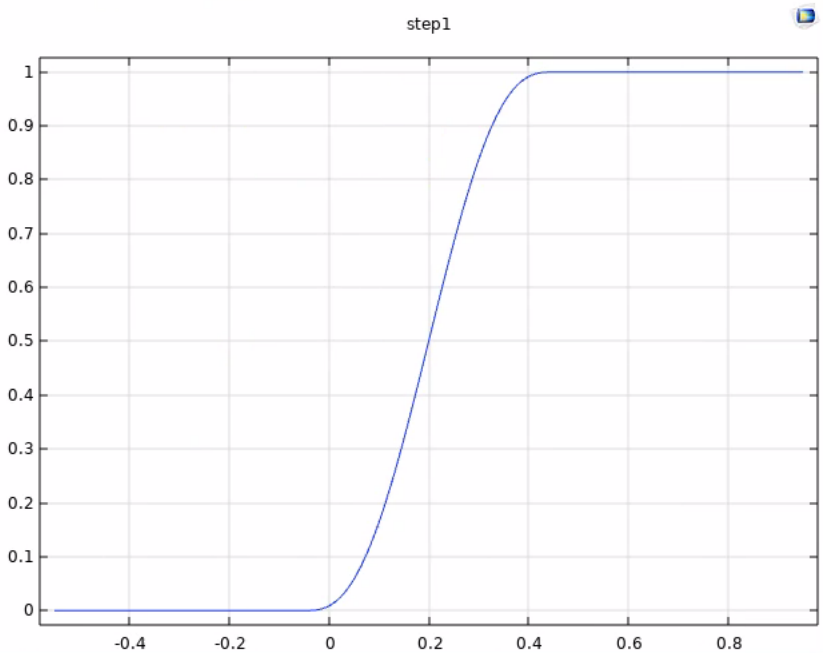

Figure 2: Visualisation of the step function step1(t) applied to the inlet pressure.

3.3.1. Phase Field

The parameter controlling interface thickness is set to pf.ep_default, The mobility tuning parameter is set to 1 ms/kg and the phi-derivative of external free energy is set to 0 J/m^3. The contact angle for the wetted wall is set to $\frac{\pi}{2}$.

3.3.2. Level Set

The reinitialization parameter is set to 15 ms^{-1} and the parameter controlling interface thickness is ls.ep_default. The factor of minimum element length is 1 and the contact angle for the wetted wall is set to $\frac{\pi}{2}$.

3.3.2 Heat Transport

The thermal conductivity, k, for a polystyrene melt is 0.23 W/mK [11]. The temperature of the mould is generally around 75 °C and the polymer melt is generally around 260 °C [12], the change in temperature that occurs to the molten polymer is then -185 °C. The initial temperature is set to 75 °C and the temperature of the fluid under the Two-phased Flow, Phase Field module is set to 260 °C. The inflow and outflow parameters are disabled, as there is no heat flow going into the system. The boundary heat source Q_b is set to -100 W m^{-2}.

4. Result and Discussion

There are many considerations when moulding a product via injection moulding. The most important aspect is complete filling of the mould. Without complete filling of a mould, the product is defective and cannot be sold. Other aspects are filling time, the shorter the filling time, the faster the cycle time, and the more products that can be made. The air vents should be engineered as such that the polymer does not flow through and with a reasonable air flow rate. All these aspects can be controlled by changing the viscosity of the polymer melt or changing the pressure applied at the inlet. This section aims to show the effect of changing the viscosity of the polymer and changing the applied pressure in the inlet on the end product.

4.1. Mesh study

In this section, the mesh analysis will be described. To optimize the model, a mesh analysis is necessary to balance accuracy of results and computational efficiency. A finer mesh yields higher accuracy but at greater computational expense. The goal is to select a mesh size that ensures reasonable accuracy while minimizing computational time. This entails running a stationary single phase flow through the model and recording the inlet pressure, outlet pressure, and outlet velocity, at different mesh sizes. The inlet velocity was set to 0.1 ms^{-1} and the outlet pressure was set to 0 Pa. The different mesh sizes and corresponding results are provided in Table 1.

Table 1: Results from the mesh analysis.

	Extremely coarse	Extra coarse	Coarser	Coarse	Normal	Fine	finer	Extra fine
Element size [mm]	4.63	2.94	2.06	1.61	1.07	0.85	0.60	0.37
1/Element size	0.22	0.34	0.48	0.62	0.94	1.18	1.67	2.68
Inlet Pressure [Pa]	$1.37 \cdot 10^6$	$1.32 \cdot 10^6$	$1.25 \cdot 10^6$	$1.14 \cdot 10^6$	$9.55 \cdot 10^5$	$1.04 \cdot 10^6$	$6.84 \cdot 10^5$	$1.42 \cdot 10^6$
Outlet Pressure [Pa]	$5.03 \cdot 10^4$	-93	$-6.15 \cdot 10^3$	$3.10 \cdot 10^4$	$2.28 \cdot 10^4$	$1.58 \cdot 10^4$	$8.15 \cdot 10^4$	$3.56 \cdot 10^4$
Outlet Velocity [ms^{-1}]	20.4	22.5	22.6	23.0	23.3	23.4	23.5	23.5

To aid visualisation, the results were plotted against the reciprocal of the element size to assess whether the results converge to a single value (Figure 3). The plot for outlet velocity shows clear convergence towards a velocity of 23.5 ms^{-1}. This plot suggests a mesh size of coarser, coarse, or normal will give reasonably accurate results. The mesh size extra fine, finer, and fine are the most similar to the convergence number, however, the difference is not that large, so a coarser mesh will

be preferable when computational cost is taken into account. The outlet pressure shows signs of convergence to a pressure of 0 Pa. The plot shows that for the coarser mesh this result was also obtained, while the results in between extra fine and coarser are not accurate. The inlet pressure does not show any convergence. The pressure at extra fine and extra coarse is the same, with the pressure at coarser being relatively similar. This analysis shows that the coarser mesh will give reasonably accurate results similar to an extra fine mesh, with a fraction of computational cost.

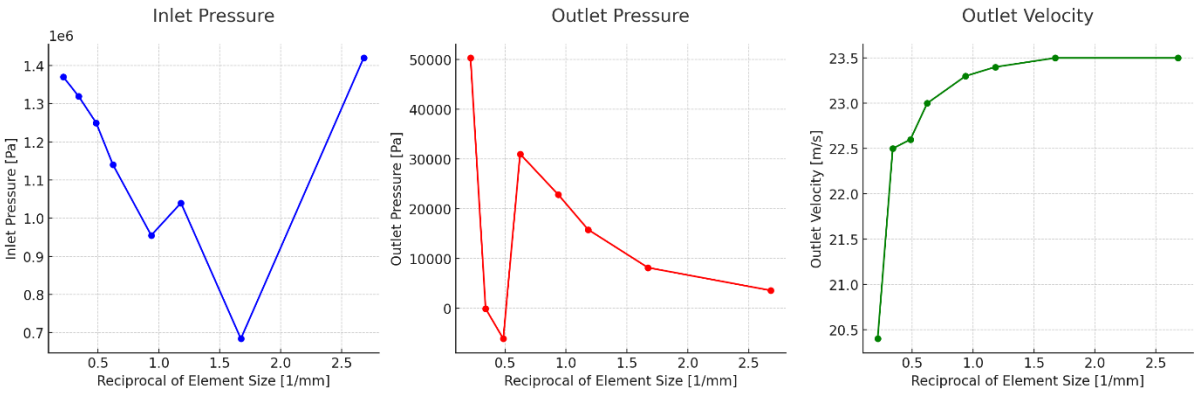

Figure 3: Results of mesh analysis plotted against the reciprocal of the element size.

4.2. Phase Field

Using the phase field method, 9 simulations were performed using pressures of 500, 600, and 600 bar, combined with a viscosity of 1, 2, 5 Pas. The volume average volume fraction over the whole domain of the mould is given in Figure 4. This graph shows the degree at which the mould is filled over time, where the volume fraction is given for air, therefore the smaller the volume fraction the less air and more filling. All 9 simulations are plotted where the colour represents a specific pressure, and the type of line represents a viscosity. The legend is labelled, for example, “600 1” meaning, a pressure of 600 bar and viscosity of 1 Pas.

It was expected for a given pressure, the higher the viscosity the more time it would take for the mould to fill, for example, that the solid lines (lowest viscosity) would be at the bottom of the graph, the dashed lined in the middle, and the dashed-dot line (highest viscosity) at the top. This general trend is only observed with the highest viscosity at 5 Pas. Interestingly, no trend is observed otherwise. Perhaps the viscosities 1 Pas and 2 Pas were not different enough to warrant an observable change in filling time. The viscosities chosen do not accurately reflect the viscosity of a polymer melt and were chosen based on numerical stability of the simulation. For future simulations, a greater difference between viscosities should be chosen. If numerical stability can be achieved, the VFT viscosity discussed in section 2.1. should be used. There is also no trend

observed with pressure, as expected that higher pressures will increase filling time, however, this is not observed for any viscosity.

What can be observed from Figure 4 is that the filling of the mould happens very quickly in all cases, where 84% is filled within 0.1 seconds, and almost complete filling (98%) of the mould happens generally within 2 seconds. It is interesting to note that there seems to be an asymptote at a volume fraction of 0.02, and an asymptote that is slightly higher for the two higher viscosity simulations. This means that the mould does not completely fill and indicates that the higher the viscosity, the more time it takes to fill. 2% space is significant in injection moulding because this will give the appearance of dents in the final product. Dog bone tensile strength samples should have minimal defects as this can result in incorrect measurements of mechanical properties. According to a study done, low viscosity polymer melts are advantageous to mould filling because of their higher contact angle, θ_w, with stainless steel [13]. The contact angle used in this simulation was 90°. According to the literature 90° is on the high side especially for viscosities this low which is practically not achieved nor desired in injection moulding of polymer melts. For future simulations, contact angles on the lower end of the scale should be chosen i.e. 70° concomitantly with the VFT viscosity to observe the effect on filling.

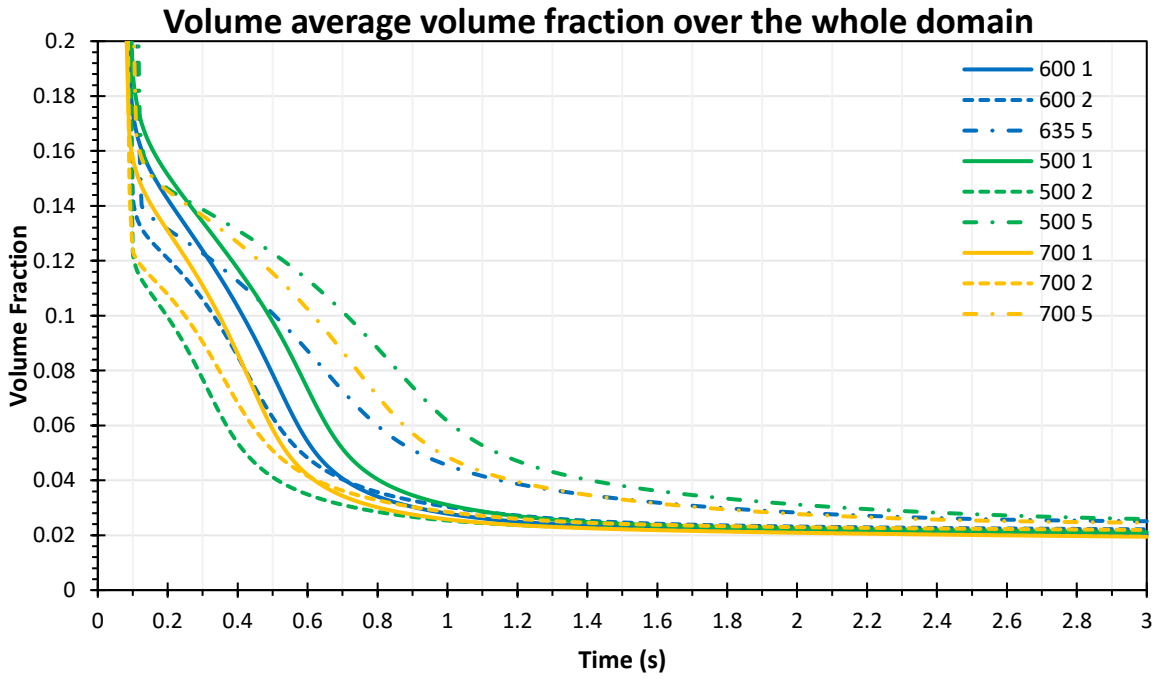

Figure 4: Volume fraction of air over the whole volume cavity of the mould. The colour represents a pressure [bar] and the type of line represents the viscosity [Pas]. The legend is read as follows "600 1" = 600 [bar] 1 [Pas].

Other than complete filling of a mould, the other major aspect of injection moulding is the prevention of polymer melts spilling out of the mould and into the air vents. Figure 5 shows the

volume fraction of the surface at the outlet over time. This graph shows that the polymer starts flowing through the vent at t = 0.1 s, and the rate at which volume increases significantly starts at around 0.5 seconds. This is to be expected from viscosities so low. What was interesting to observe in this case is whether there is a difference between pressures and viscosities on the outflow of the polymer melt. From the graph, there is no trend to be observed for the lower viscosities, but there is for the polymer melt of viscosity 5 Pas. From the previous figure it showed that the mould cavity was essentially completely filled by 2 seconds, it is expected that by this time the outflow is mainly comprised of polymer. Generally this is the case aside from the high viscosity polymers which have a significant amount of delay before it exists the vent. It is also interesting to observe that the high viscosity with higher applied pressure, exits the vent faster than the one wit lower pressure. This is to be expected. In practice of course the viscosities are much higher, and the air vent are engineered such that the polymers do not protrude it, therefore for future simulations it would be interesting to observe if using the VFT viscosity will improve this.

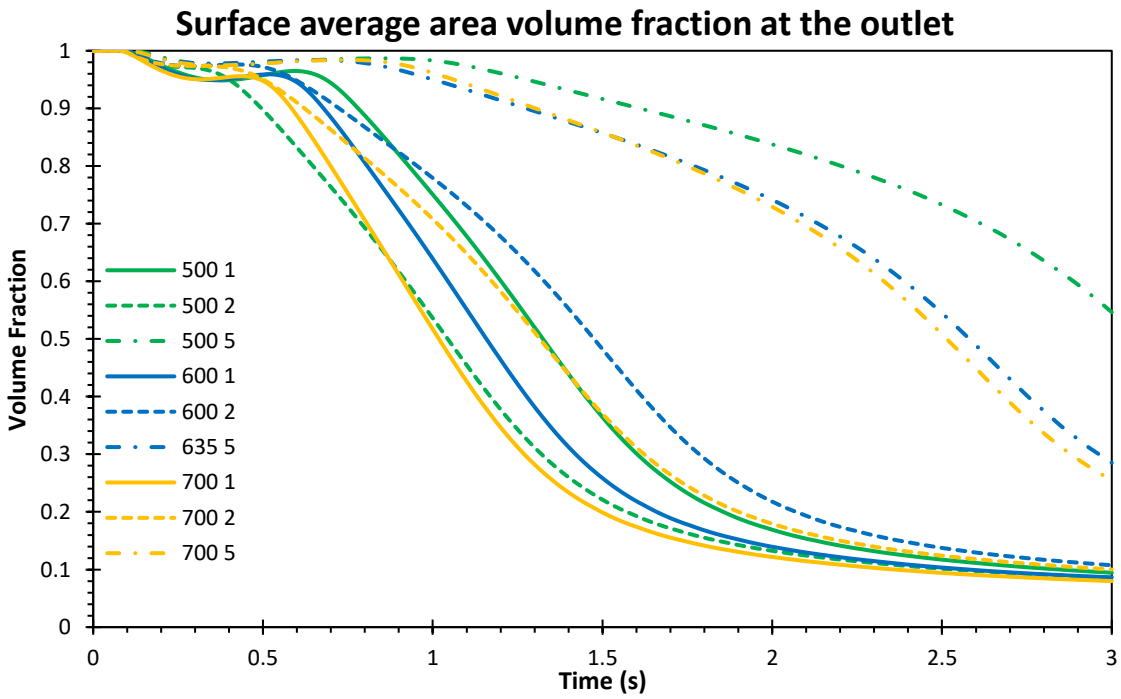

Figure 5: Plot of the surface average volume fraction of air in the outlet. The colour represents a pressure [bar] and the type of line represents the viscosity [Pas]. The legend is read as follows "600 1" = 600 [bar] 1 [Pas].

4.3. Comparison of Phase Field (PF) with the Level Set method (LS)

In this section the observed differences between Phase Field (PF) and Level Set method (LS) will be discussed. Both methods can be used for tracking the interface for a two phased flow. Figure 6 shows the direct comparison of how the mould is filled over time between the two methods. First

thing to note is that the phase field method has numerical instability with a pressure of 600 bar and a viscosity of 5 Pas, this simulation could not converge. Convergence only occurred when the pressure became above 635 Pa. The level set method did not have any issues with convergence. In the PF method the rate of filling slows dramatically at a volume fraction of air of 0.16 – 0.18 and almost has a linear downward slope before being almost completely filled at volume fraction of 0.04. The LSM follows an exponential decay trend and only slows down when the volume fraction reaches 0.06. The LSM volume fraction also continues to decrease over time while the PF method seems to stop decreasing after around 2 seconds. Figure 7 shows what the observed filling is over time for the phase field method.

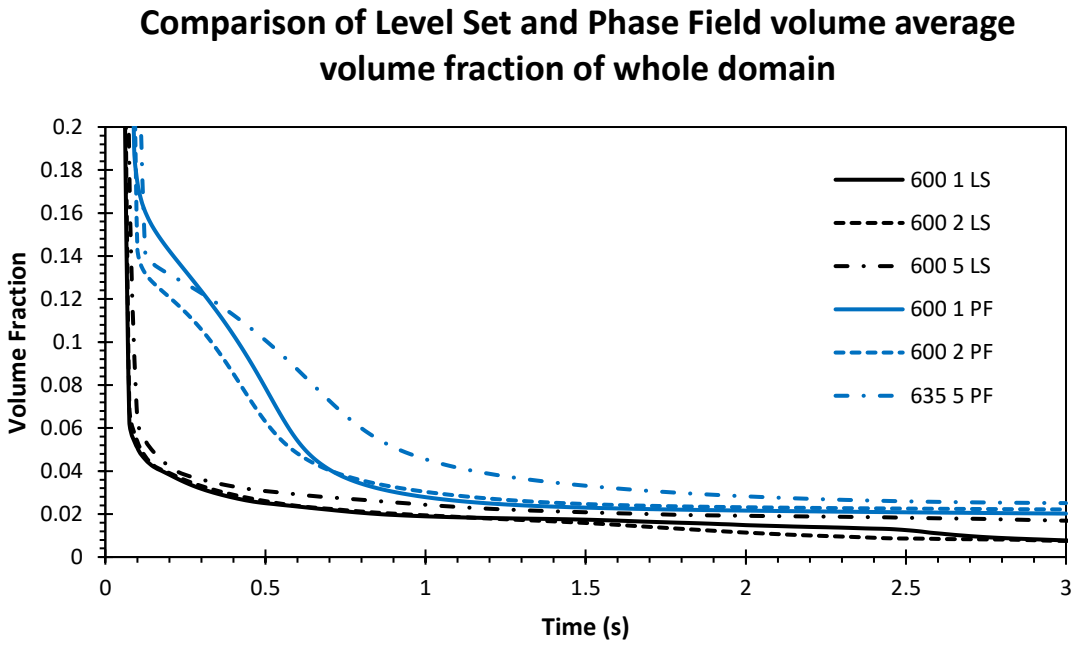

Figure 6: Graph comparing the PF to LS of the volume average volume fraction. The colour represents the method; blue = Phase Field (PF) and black = Level Set (LS). The type of line represents the viscosity [Pas]. The legend is read as follows "600 1" = 600 [bar] 1 [Pas] Level Set.

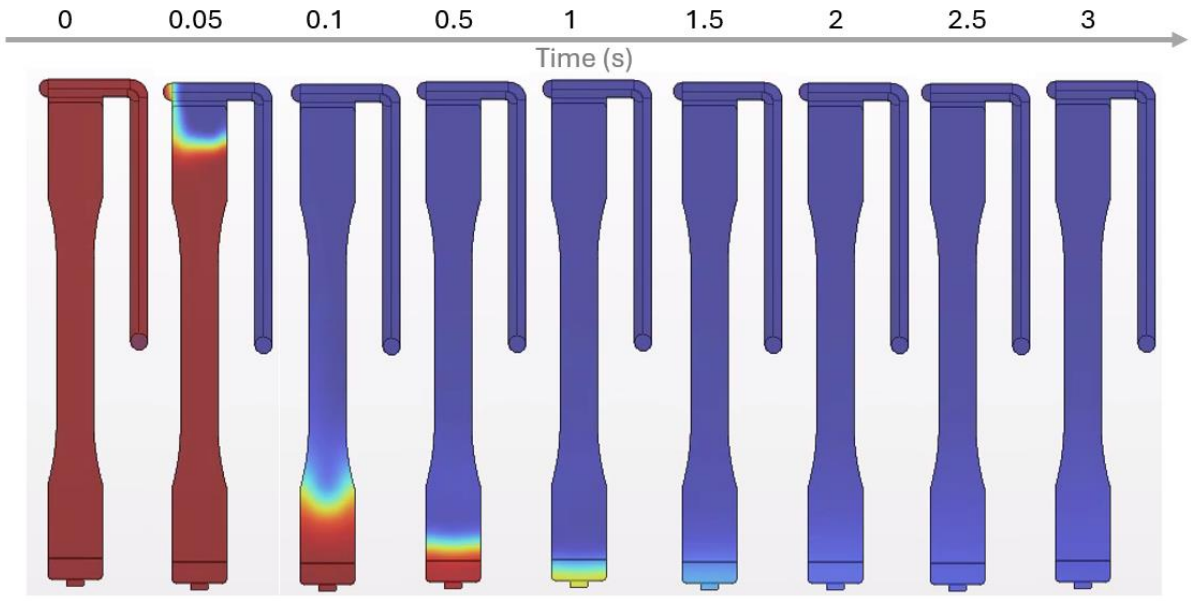

Figure 7: Observed filling over time for the phase field method.

Visually, the two methods appear quite different in how they fill. For example, compare Figure 7 and Figure 8 which shows how the filling of the mould over time. The PF method has a much more structured filling than the LS method. In the LS method there are air pockets along the side and in the corners, while in the PF method the interface remains a straight line across the width of the domain.

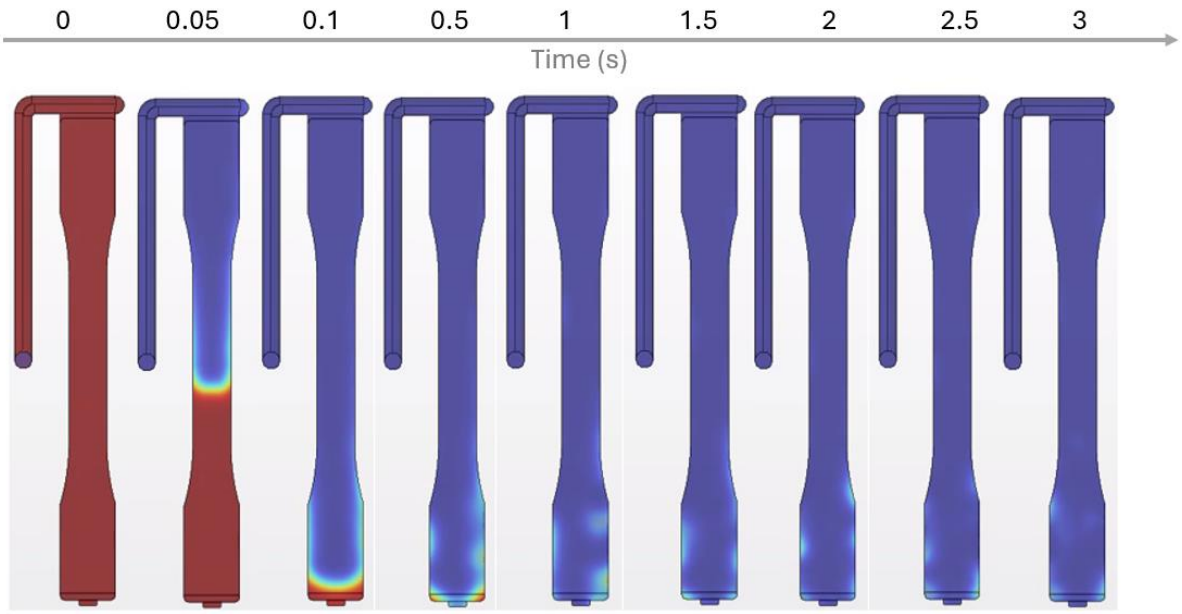

Figure 8: Observed filling over time for the level set method.

At 2 seconds, again the LS method has some air pockets that slowly disappear over time. In the PF method there are no air pockets along the sides, the air volume fraction evenly reduces towards the end.

Figure 9 shows the difference in the outlet volume fraction. The outlet volume fraction of the PF method has a very smooth transition, which corresponds with what was observed visually. The LS method the downward trend is clear but there is a lot of back and forth. Another thing to note is that the downward trend does not have the same shape, the PF has a more sigmoidal shape while the LS method has an exponential decay shape.

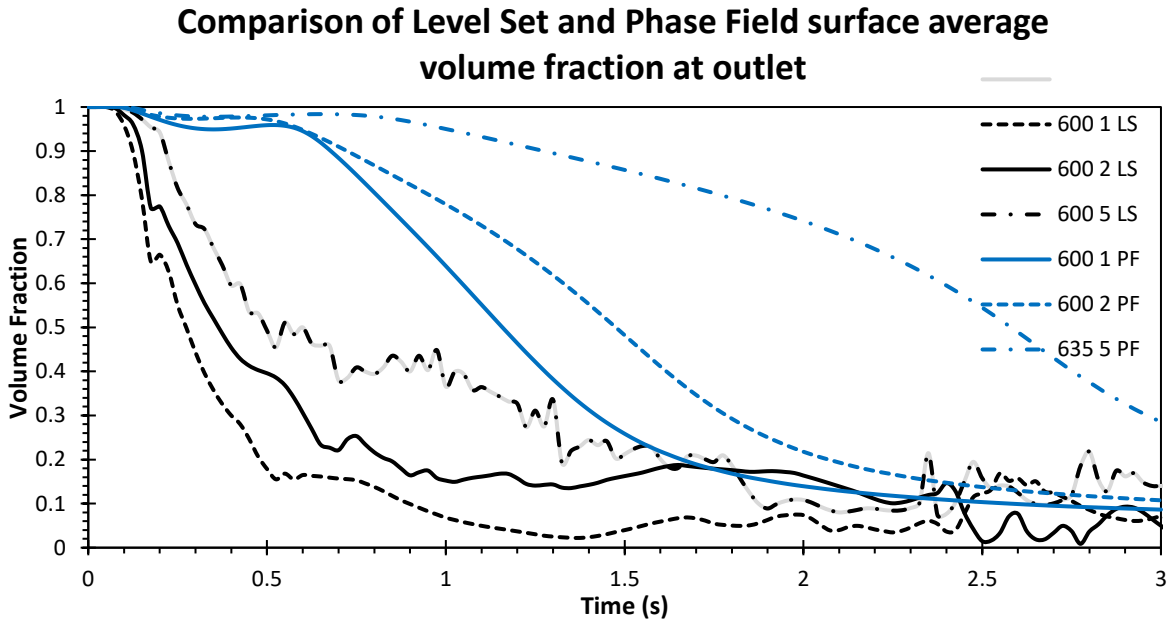

Figure 9: Comparison of the Level Set (LS) method and Phase Field (PS) method surface average volume fraction at the outlet. The legend is read as follows "600 1" = 600 [bar] 1 [Pas] Level Set.

Since there is no direct empirical data to compare to, no conclusive comment can be made about the accuracy of either of the methods. In general, in injection moulding, the evolution of air pockets in the mould does happen when the processing conditions are not optimized, therefore perhaps the LS method was able to capture that more accurately, but this is difficult to say without empirical data. The LS does offer some advantages over the PF method as it showed numerical stability over all the pressures and viscosities that were tried, while the PF method had some convergence issues with certain values.

4.4. Heat Transfer

This section will describe the results of adding the Heat Transfer in Fluids module to the phase field two phased flow module. The simulation was able to converge, however, currently the model is not sufficient to provide meaningful results due to the limitations of the program. In injection moulding, the hot molten polymer is shot into the mould upon where it rapidly cools. The parameters that define how much the polymer melt cools is the temperature of the mould and the

temperature of the polymer melt. These parameters cannot be set in the program the change in temperature of the polymer melt over time cannot be observed accurately. The only option in the program is to set the heat flux leaving the system. This was set arbitrarily to -100 W m^{-2}, for the purposes of this report the exact value is not important, only that there is some kind of cooling effect in the system. The temperature of the polymer melt entering the system cannot be set.

Running the simulation with these parameters give results that cannot be interpreted in any way. Initially, the temperature cools slightly throughout the mould (as there is -100 Wm^{-2} leaving the system). At t = 1.5 s, where the mould is filled 70%, the temperature in the first half of the mould is on the order of 10^2 K, and the temperature in the second half of the mould is in the negative Kelvin (Figure 10). In the air vent the temperature is on the order of 10^4 K, even though the temperature change due to viscous dissipation is not included.

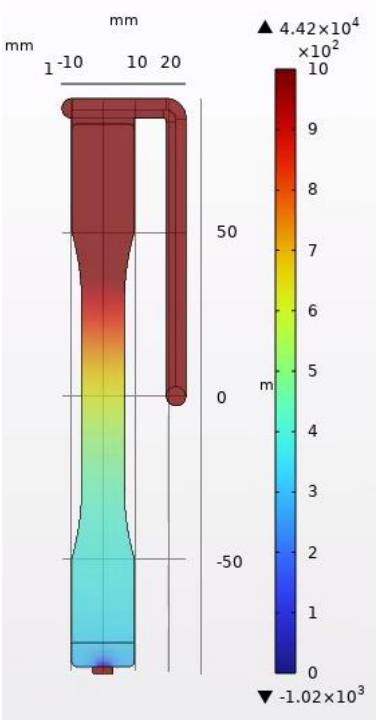

Figure 10: Temperature profile of the mould at t = 1.5 s where the mould has been filled 70%.

4.5. Limitations

This section will discuss the limitations of this project. The velocity at the outlet of the mould was recorded over time, shown in Figure 11. The velocities at the outlet is far too high. In fact, they are completely unreasonable and velocities like this can cause serious air compression and superheating which can cause the polymer to spontaneously combust. This is termed to “diesel” [14]. The parameters chosen for this project such as the geometry of the mould, the air vents and the applied pressure all match that what is used in practice. The only change is the polymer

viscosity. Generally polymer viscosities are much higher. From the previous graphs it was observed that the higher viscosity polymers have a slower filling time, and this is evident in Figure 11 as the velocity at the outlet is significantly lower. It is estimated that if a polymer viscosity of 1500 Pas is used, the velocity range will be much more reasonable.

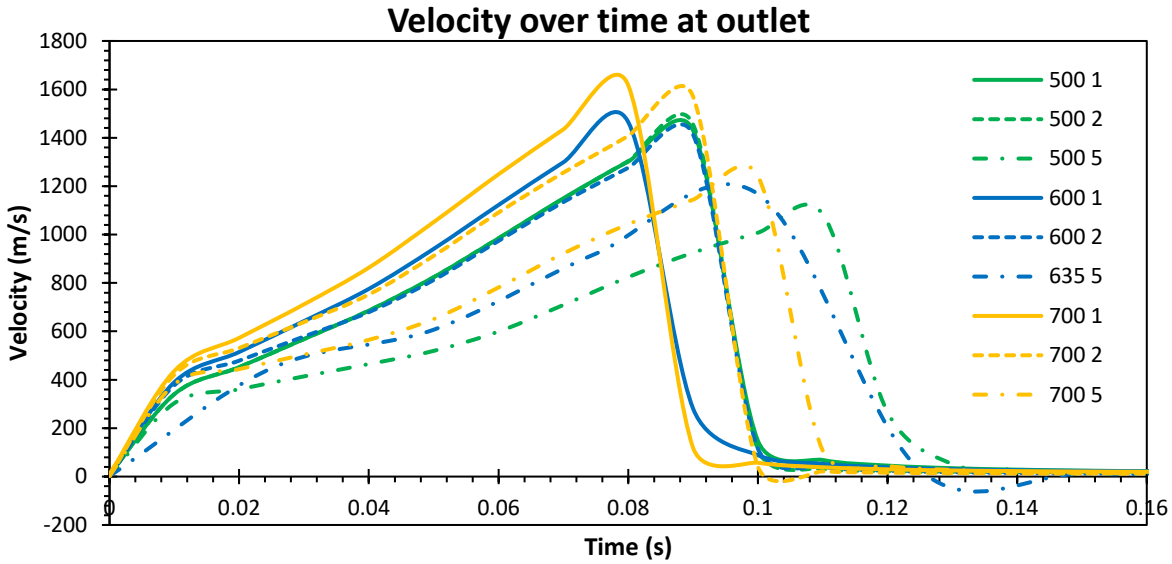

Figure 11: Velocity at the outlet of the mould. The colour represents a pressure [bar] and the type of line represents the viscosity [Pas]. The legend is read as follows "600 1" = 600 [bar] 1 [Pas].

There were some limitations in the heat transfer model as well. Because the velocities are so high, this causes increased amounts of viscous dissipation, where the temperatures would reach over 10^4 K, which is completely false. Again, this is likely due to the excessively fast filling time due to the low viscosity. Filling times can be upwards of 1 second, rather than 0.1 s.

Another aspect of heat transfer is that the only option given is the input for a heat sink, as explained in the previous section. This means that heat is withdrawn from the air initially present in the mould and that there is constant heat withdrawal as the mould is filled. This does not reflect reality as the mould is at a constant temperature, therefore the air that is room temperature first heats up, and as the polymer melt is injected, it rapidly cools down. The cooling would slow as the polymer cools as well due to decrease in driving force (ΔT). The air temperature can be considered negligible, and therefore it is ignored in this project, however, the change of heat flux leaving the polymer melt is significant. The other aspect to this is that the polymer melt viscosity changes significantly as it cools down, and it should solidify once it reaches its melting temperature of 240 °C [15]. For future simulations, other modules in COMSOL should be utilised to emulate phase change with change in temperature.

5. Conclusion

This study's examination of the phase field (PF) and level set (LS) methods in simulating the injection moulding process reveals distinct behaviours and outcomes associated with each technique. The simulations conducted using different pressures and viscosities demonstrated that, while there is a general expectation that higher viscosities lead to slower mould filling, this trend was only clear with the highest viscosity values tested. The negligible difference observed between the lower viscosities suggests a need for a broader range of viscosity values in future studies to capture more nuanced effects. The phase field method showed numerical instability at certain pressure and viscosity settings and also an apparent stop in volume fraction decrease after a certain point, an issue not encountered with the level set method, indicating a potential advantage of the LS method in handling a greater range of simulation conditions. Additionally, the PF method exhibited a more structured filling pattern, maintaining a straight interface across the mould, unlike the LS method, which showed air pockets and a less uniform filling pattern. For future research, incorporating a wider range of viscosity values and possibly employing the Vogel-Fulcher-Tammann (VFT) viscosity model could provide more insight into the mould filling process. Additionally, exploring lower contact angles could offer a more realistic simulation of polymer melt behaviour in injection moulding. Overall, this study underscores the importance of selecting an appropriate simulation method based on the specific requirements and conditions of the injection moulding process. While the PF method offers advantages in terms of filling uniformity and smooth outflow transitions, the LS method provides better stability under a broader range of conditions, highlighting the trade-offs that must be considered in the choice of simulation techniques.

Heat transport was added to the simulation to emulate to cooling effect of the mould on molten polymer melt, the simulation converged, but the results are not meaningful due to limitations in the program. Specifically, the inability to set critical temperature parameters for the polymer melt and the mould in the injection moulding simulation leads to unrealistic temperature distributions, such as negative Kelvin values. Consequently, the current model requires significant improvements to provide accurate and interpretable results for injection moulding processes.

References

[1] S. Littmarck and F. Saeidi, “COMSOL Multiphysics 6.0 [software],” 2021. [Online]. Available: https://www.comsol.com.

[2] A. A. Miller, “Analysis of the Melt Viscosity and Glass Transition of Polystyrene,” *Journal of Polymer Science,* vol. 6, pp. 1161-1175, 1968.

[3] G. K. Batchelor, An Introduction To Fluid Dynamics, Cambridge: Cambridge University Press, 1967, pp. 142-148.

[4] J. Pedlosky, Geophysical Fluid Dynamics, 2 ed., Springer, 1990.

[5] “Level Set and Phase Field Equations,” COMSOL, [Online]. Available: https://doc.comsol.com/5.5/doc/com.comsol.help.cfd/cfd_ug_fluidflow_multi.09.094.html. [Accessed 03 2024].

[6] “The Level Set Method,” COMSOL, [Online]. Available: https://doc.comsol.com/6.0/doc/com.comsol.help.cfd/cfd_ug_math_levelset_phasefield.14.33.html#1811600. [Accessed 03 2024].

[7] “The Heat Transfer iin Fluids Interface,” COMSOL, [Online]. Available: https://doc.comsol.com/6.2/docserver/#!/com.comsol.help.heat/heat_ug_interfaces.08.32.html?type=ext. [Accessed 03 2024].

[8] “SOLIDWORKS,” Dassault Systemes, 2000. [Online]. Available: https://www.solidworks.com/. [Accessed 01 2024].

[9] “ASTM D638 TYPE I,” [Online]. Available: https://axxicon.com/product/astm-d638-type-i-pcf0009/.. [Accessed 01 2024].

[10] “The Materials Analyst, Part 69: Density, bulk density, melt density, and specific gravity (Web-exclusive),” 01 01 2006. [Online]. Available: https://www.plasticstoday.com/injection-molding/the-materials-analyst-part-69-density-bulk-density-melt-density-and-specific-gravity-web-exclusive-. [Accessed 02 2024].

[11] A. Dawson and M. Rides, “Thermal conductivity of polymer melts and implications of uncertainties in data for process simulation,” Division of Engiineering and Process Control, Teddington.

[12] “PS (Polystyrene),” [Online]. Available: https://www.fastheatuk.com/mdb/ps.html. [Accessed 03 2024].

[13] G. Zitzenbacher, H. Dirnberger, M. Längauer and C. Holzer, “Calculation of the Contact Angle of Polymer Melts on Tool Surfaces from Viscosity Parameters,” *Polymers,* vol. 10, no. 1, p. 38, 2017.

[14] J. Fattori, “Back to Basics on Mold Venting (Part 1),” 3 18 2019. [Online]. Available: https://www.ptonline.com/articles/part-1-back-to-basics-on-mold-venting. [Accessed 03 2024].

[15] J. Wunsch, in *Polystyrene - Synthesis, Production and Applications*, Shrewbury, iSmithers Rapra Publishing, 2000, p. 15.

[16] H. V. d. Akker and R. F. Mudde, Transport Phenomena, Delft: Delft Academic Press, 2014.

[17] S. Sato, K. Oka and A. Murakami, “Heat transfer behavior of melting polymers in laminar flow field,” *Polymer Engineering and Science,* vol. 44, no. 3, p. 423, 2004.

[18] “Injection Molding Machine : Construction, Working, Application, Advantages and Disadvantages,” [Online]. Available: https://www.cewheelsinc.com/injection-molding-machine-construction-working-application-advantages-disadvantages/. [Accessed 03 2024].